IEEE Access
Multidisciplinary | Rapid Review | Open Access Journal

Received December 31, 2019, accepted January 20, 2020, date of publication February 3, 2020, date of current version February 12, 2020.

Digital Object Identifier 10.1109/ACCESS.2020.2971002

Estimating the State-of-Charge of Lithium-Ion Battery Using an H-Infinity Observer Based on Electrochemical Impedance Model

NING CHEN, PENG ZHANG, JIAYANG DAI, AND WEIHUA GUI
School of Automation, Central South University, Changsha 410083, China

Corresponding author: Jiayang Dai (daijiayang@csu.edu.cn)

This work was supported by the Foundation for Innovative Research Groups of the National Natural Science Foundation of China under Grant 61621062.

ABSTRACT The lithium-ion batteries in the electric vehicles are nonlinear systems with complex electrochemical dynamics, and estimation of battery state-of-charge (SOC) is affected by factors such as environmental temperature and battery current. Considering the above problems, the accurate estimation of battery SOC has always been a difficult and the critical issue of battery management system (BMS). In this paper, the constant phase element (CPE) is introduced to the traditional time domain circuit model by analyzing the electrochemical impedance spectra of lithium-ion batteries. Accordingly, an equivalent circuit model based on electrochemical impedance is constructed by using fractional order theory, which has specific physical significant, leading to the improved estimation accuracy to represent battery voltage. Moreover, the polarization resistance in the model is replaced by Butler-Volmer (BV) equation, which can solve the problem caused by large current and temperature variation during the actual operation of electric vehicles. Next, based on the model, an H∞ observer is designed for battery SOC estimation, and the proposed SOC observer is tested by real-time experimental data of battery. The efficiency of the proposed model and observer are validated by some simulations and experiment tests.

INDEX TERMS Lithium-ion batteries, Butler-Volmer equation, state of charge estimation, electrochemical impedance model, fractional calculus, H∞ observer.

I. INTRODUCTION

With the promotion of renewable energy, more and more attention has been paid to electric vehicles [1], [2]. Electric vehicles have many advantages: environment-friendly, clean energy, low cost investment. However, low performance of the BMS of electric vehicle is still the most essential restriction for the development of electric vehicle, and estimation of battery SOC is one of the main functions of the BMS. SOC is defined as the percentage of the amount of left energy to the rated capacity of a battery, which cannot be measured directly, and can only be estimated by the indirectly measured variables such as current and terminal voltage [3]. Considering battery internal performance and the diversity of operating conditions, the high-precision estimation of battery residual SOC is still a great challenge [4], [5]. Inaccurate estimation of the SOC may lead to over-charge and over-discharge of the battery, which affects the safety and life of the battery. Hence, high-precision estimation of the SOC is necessary [6].

A large number of scholars have proposed a variety of SOC estimation methods: ampere-hour integral method, data-driven estimation method, model-based method and so on. Among them, the ampere-hour integral method is the most commonly used method in the laboratory, however, due to the accumulation of the measurement errors of battery current, the ampere-hour integral method will lead to large estimation error of the SOC, this method is more apt to work as the supporting technique of other methods. Shen proposed a novel approach using adaptive artificial neural network (ANN)-based model and neuro-controller for SOC estimation, results show that the ANN-based battery system model adaptively simulates battery system with high accuracy, and the predicted SOC converges to the real value quickly within the error of 1% [7]. However, the data-driven

The associate editor coordinating the review of this manuscript and approving it for publication was Xiaosong Hu.

This work is licensed under a Creative Commons Attribution 4.0 License. For more information, see http://creativecommons.org/licenses/by/4.0/

method may not even be convergent with bad parameters selection when the training data cannot completely cover the present operating conditions [8]. Estimators or observers provide an effective method to estimate SOC. Some schemes such as the state observer [9]–[12], Kalman filter [13]–[16], particle filter [17], [18] and H∞ observer [19], [20] are the most commonly used methods for SOC estimate. Performance of an observer is dependent on the quality of a dynamic model of the lithium-ion batteries, and many models have been applied to estimate the SOC of lithium-ion batteries. Generally, common models can be classified into three categories: electrochemical model, equivalent circuit model and electrochemical impedance model. Han *et al.* [21] developed a simplified pseudo-two-dimensional (SP2D) model, which could simulate the battery efficiently without too much loss of accuracy. Base on this model, an estimation algorithm using the Luenberger observer is proposed. Although electrochemical model can describe the mechanism of the BMS, it is difficult to identify all parameters. In addition, it requires the specialized know-how of the operator. Chen and Rincon-Mora [22] proposed an accurate, intuitive and comprehensive equivalent circuit model by considering all the dynamic characteristics of the battery, the proposed model can accurately predict the running time and performance of the battery. However, the more RC modules in the equivalent circuit, the higher accuracy of the model, it will also lead to increase of model parameters and computational burden. Xiong *et al.* [23] proposed a BV equation-based fractional order model for electric vehicle, and it is proved that it has good performance concerning the terminal voltage estimation accuracy and SOC estimation accuracy. Since the diffusion between the internal electrodes of lithium-ion batteries belongs to a typical type of anomalous diffusion based on fractal medium, the diffusion coefficient is directly related to the fractional-order, the physical significance of the electrochemical impedance model based on the fractional order theory is clear, and the electrochemical impedance model combines the accuracy of electrochemical model and the adaptability and extensibility of equivalent circuit model, it may describe the inherent characteristics of lithium-ion battery. This paper will investigate the SOC estimation method based on the electrochemical impedance model.

To accurate estimate the SOC of lithium-ion batteries in electric vehicles, an H∞ observer is proposed based on a novel equivalent circuit model of electrochemical impedance. In Section II, the model which considers both BV equation and CPE is proposed. Section III proposes the H∞ observer for SOC estimation. Section IV introduces the battery test system and the characteristic test of battery. Experimental results and discussions are provided in Section V. The conclusions are presented in the last Section.

II. BATTERY ELECTROCHEMICAL IMPEDANCE MODEL

A. ELECTROCHEMICAL IMPEDANCE MODEL

Electrochemical impedance spectroscopy (EIS) is an important tool for analyzing the dynamic behavior of battery.

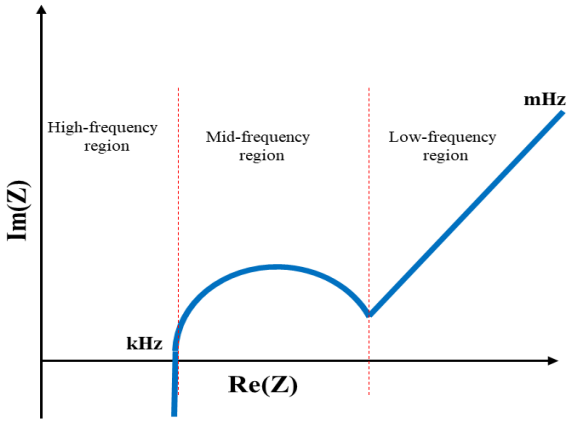

FIGURE 1. Typical EIS of the lithium-ion battery.

EIS is one of the accurate methods for simulating lithium-ion batteries, many studies attempt to estimate SOC directly by EIS, but the EIS method is too complicated to be applied directly. At present, EIS is mainly used to establish electrochemical impedance circuit model.

The EIS of a lithium-ion battery can be divided into three parts: high-frequency region, mid-frequency region and low-frequency region. A typical lithium-ion battery EIS is shown in Fig. 1, in which the horizontal axis is the real part of the impedance and the vertical axis is the imaginary part of the impedance. In the high-frequency region, the EIS curve intersects the real axis, and the intersection point represents the ohmic resistance of lithium battery. In the mid-frequency region, the EIS curve is a semi-circular curve segment, which is related to the double electric layer at the interface between the battery electrode and electrolyte. This characteristic is described by parallel connection of a resistor and a CPE. In the low-frequency region, EIS curve is a straight line with constant slope associated with the solid diffusion process inside the lithium-ion active material particles, which is described by CPE. In the EIS analysis, fractional-order components such as CPE are often used instead of ordinary RC component in order to get higher accuracy. Therefore, to make the model more accurate by replacing two capacitors in the common second-order RC circuit model with fractional-order components, the equivalent circuit model of electrochemical impedance shown in Fig.2 can be obtained.

In Fig.2, the circuit impedance of CPE_1, and CPE_2 can be expressed as

$$Z_{\mathrm{CPE1}}(j\omega) = \frac{1}{Y_1 \cdot (j\omega)^{r_1}} \quad (0 < r_1 < 1)$$
$$Z_{\mathrm{CPE2}}(j\omega) = \frac{1}{Y_2 \cdot (j\omega)^{r_2}} \quad (0 < r_2 < 1) \qquad (1)$$

where $Y_1, Y_2 \in \mathbf{R}$ represent the coefficient of the CPE; j is an imaginary unit; $\omega = 2\pi f, f$ is the frequency; V_{oc} denotes open circuit voltage (OCV); V_h is battery terminal voltage which can be directly measured; R_a, R_b and R_c represent the Ohmic resistance; V_b and V_c denote the terminal voltage

of CPE_1 and CPE_2; r_1, r_2 are the arbitrary order of the fractional element. $0 < r_1 < 1$ and $0 < r_2 < 1$ represent respectively the extent to which CPE_1, CPE_2 deviates from pure capacitive element. When $r_1 = r_2 = 0$, CPE_1 and CPE_2 are equivalent to resistors; when $r_1 = r_2 = 1$, CPE_1 and CPE_2 are equivalent to capacitors. The size of r_1 determines the distance from the center of the arc to the real axis in the mid-frequency of the EIS curve in Fig.1, and r_2 determines the slope of the straight line in the low-frequency section of the curve [24].

B. DEFINITIONS FOR FRACTIONAL CALCULUS

Through the analysis of EIS, CPE can well describe the electrochemical impedance characteristics of battery, which can be applied to battery model establishment and state estimation. However, the CPE is difficult to deal with in time domain which need to be processed by means of fractional calculus theory.

Fractional calculus is an extension of the traditional integer calculus, first proposed by Leibniz in 1695, and has now become a hot research topic in the field of science and engineering. Fractional calculus has high accuracy in describing nonlinear systems such as battery [25]. In fractional calculus, the operator ${}_aD_t^r$ defined as (2), where ${}_aD_t^r$ is used to represent the derivative or integral of arbitrary order r with respect to t; a is the initial time, here, a is 0 by default in this paper. When $r > 0$, ${}_aD_t^r$ represents the fractional derivative; when $r < 0$, it stands for the fractional integral. We consider only $0 < r < 1$, and the operator is then simplified as D^r.

$$aD_t^r = \begin{cases} \dfrac{d^r}{dt^r}, & r > 0 \\ 1, & r = 0 \\ \displaystyle\int_a^t (d\tau)^{-r}, & r < 0 \end{cases} \tag{2}$$

The Grünwald–Letnikov (G-L) definition is one of the most commonly used definitions [26], the fractional order G-L definition is defined as

$$d^r f(t) = \lim_{T_h \to 0} \frac{1}{T_h{}^r} \sum_{q=0}^{[t/T_h]} (-1)^q \binom{r}{q} f(t - qT_h) \tag{3}$$

where T_h is the sampling period; $[t/T_h]$ is the integer part of t/T_h; $\binom{r}{q}$ is the quadratic coefficient of Newton, shown as

$$\begin{aligned} \binom{r}{q} &= \frac{\Gamma(r+1)}{\Gamma(q+1)\Gamma(r-q+1)} \triangleq \frac{r!}{q!(r-q)!} \\ &= \frac{r(r-1)\cdots(r-(q+1))}{q!} \end{aligned} \tag{4}$$

C. INTRODUCING BV EQUATION TO ELECTROCHEMICAL IMPEDANCE MODEL

The equivalent circuit model of electrochemical impedance obtained in previous section is shown in Fig.2. Considering the wide range variation of current and significant change of temperature during the actual operation of electric vehicles,

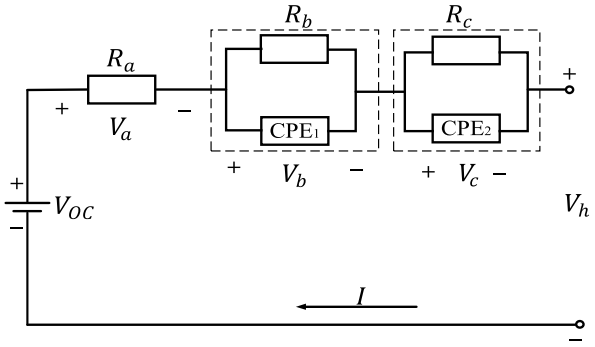

FIGURE 2. Equivalent circuit model of electrochemical impedance.

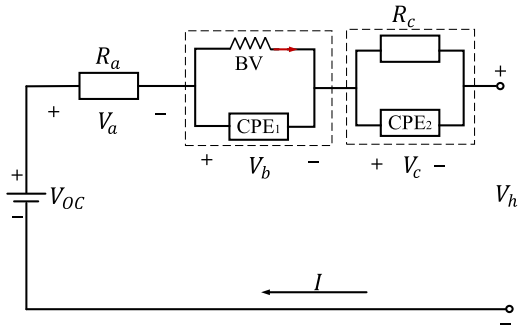

FIGURE 3. Equivalent circuit model of electrochemical impedance with BV equation.

the equivalent circuit model by replacing polarization resistance with BV equation is shown in Fig. 3.

The BV equation depicts the relationship of overpotential and current in a charge transfer process, the resistance R_b in the circuit model is replaced by BV equation as

$$I_R = k_J \cdot \left(exp\left(\frac{a_a \cdot n \cdot F}{R_g \cdot T} \cdot V_b \right) - exp\left(\frac{-a_c \cdot n \cdot F}{R_g T} \cdot V_b \right) \right) \tag{5}$$

where I_R denotes the current; V_b denotes the polarization voltage. k_J is the product of exchange current density and electrode area; a_c and a_a are cathodic and anodic charge transfer coefficients ($a_c + a_a = 1$, a_c, $a_a > 0$); n is the number of electrons involved in the electrode reaction; F is the Faraday constant(96485C· mol-1); R_g is the universal gas constant (8.314J· $mol^{-1} \cdot K^{-1}$); T stands for temperature in K.

The cathodic and anodic charge transfer reaction coefficients to be equal($a_c = a_a$), which is quite correct for lithium-ion battery [27]. Using substitutions $K(T) = a_a \cdot n \cdot F / R_g \cdot T$, the BV equation can be denoted as

$$I_R = 2k_J \cdot \left(\frac{\exp(K(T) \cdot V_b) - \exp(-K(T) \cdot V_b)}{2} \right) \tag{6}$$

Applying the definition of the hyperbolic sine function $\sinh x = \left(e^x - e^{-x}\right)/2$, (6) can be simplified as

$$I_R = 2k_J \sinh[K(T) \cdot V_b] \tag{7}$$

The mathematical model of the equivalent circuit model is established as follows

$$V_a = R_a I \tag{8}$$

$$D^{r_1} V_b = \frac{I}{Y_1} - \frac{V_b}{Y_1 R_b} \tag{9}$$

$$D^{r_2} V_c = \frac{I}{Y_2} - \frac{V_c}{Y_2 R_c} \tag{10}$$

By substituting BV equation into (9), we have

$$D^{r_1} V_b = \frac{I}{Y_1} - \frac{2k_J}{Y_1} \sinh[K(T) \cdot V_b] \tag{11}$$

Taylor expansion of $\sinh[K(T) \cdot V_b]$ in (11) is

$$\sinh [K\ (T) \cdot V_b] = [K\ (T) \cdot V_b] + \frac{[K\ (T) \cdot V_b]^3}{3!} + \frac{[K\ (T) \cdot V_b]^5}{5!} + \frac{[K\ (T) \cdot V_b]^7}{7!} + \ldots \tag{12}$$

Since V_b is a very small value, the higher order term in the expansion tends to zero and is often ignored, (11) can be simplified to

$$D^{r_1} V_b = \frac{I}{Y_1} - \frac{2k_J K(T)}{Y_1} V_b \tag{13}$$

Therefore, the model shown in Fig.3 can be described by

$$\begin{cases} V_h = -V_b - V_c - R_a I + V_{oc} \\ D^{r_1} V_b = \dfrac{I}{Y_1} - \dfrac{2k_J K(T)}{Y_1} V_b \\ D^{r_2} V_c = \dfrac{I}{Y_2} - \dfrac{V_c}{Y_2 R_c} \end{cases} \tag{14}$$

According to the formula of ampere-time integral method, we have

$$SOC = SOC_0 - \frac{1}{Q_N} \int_{t_0}^{t} \eta I dt \tag{15}$$

Differentiating (15), the fractional model of the SOC can be obtained as

$$\frac{dSOC}{dt} = D^1 SOC = -I \frac{\eta}{Q_N} \tag{16}$$

where η is the charging/discharging efficiency and Q_N is the nominal battery capacity.

Consequently, the battery is modeled as a nonlinear fractional system, which can be expressed as

$$\begin{cases} D^r x\ (t) = Ax\ (t) + Bu\ (t) \\ y(t) = Cx\ (t) + Du\ (t) + h\ (x\ (t)) \end{cases} \tag{17}$$

where $x(t) = [V_b(t) V_c(t)\ SOC(t)]^{\mathrm{T}}$ is the state vector; $y(t)$ is the battery terminal voltage V_h (system output); $u(t)$ represents the battery current I (system input); $r = [r_1 r_2 1]^{\mathrm{T}}$ represents the order vector, and A, B, C, D are the matrices with appropriate dimensions as

$$A = \begin{bmatrix} \dfrac{2k_J K(T)}{Y_1} & 0 & 0 \\ 0 & -\dfrac{1}{Y_2 R_c} & 0 \\ 0 & 0 & 0 \end{bmatrix}, \quad B = \begin{bmatrix} \dfrac{1}{Y_1} \\ \dfrac{1}{Y_2} \\ -\dfrac{\eta}{Q_N} \end{bmatrix}$$

$$C = \begin{bmatrix} -1 & -1 & d_1 \end{bmatrix}, \quad D = -R_a \tag{18}$$

The function $h^*(x(t))$ has been extensively used to represent the OCV-SOC relationship for many batteries [22], which is expressed as

$$h^*\ (x\ (t)) = \sum_{k=0}^{M} d_k SOC\ (t)^k \tag{19}$$

where $d_k (k = 0, 1, \ldots M)$ are the coefficients of $h^*(x(t))$.When the linear term $d_1 SOC(t)$ is excluded from $h^*(x(t))$ and incorporated into the input matrix C, $h(x(t))$ in (17) can be get. According to the relationship between the OCV- SOC of the battery, $h(SOC)$ is a monotonic increasing function, it can be easily shown that (19) is Lipschitz continuous within $0 \le SOC \le 1$, then $\beta_{min} \le \dot{h}\ (SOC) \le \beta_{max}$.

Since the battery charge-discharge process involves complicated physical and chemical reactions, (17) are further rewritten as (20)

$$\begin{cases} D^r x\ (t) = Ax\ (t) + Bu\ (t) + E\omega_x(t) \\ y\ (t) = Cx\ (t) + Du\ (t) + h\ (x\ (t)) + F\omega_y(t) \end{cases} \tag{20}$$

where ω_x denotes the state disturbance; ω_y is the output disturbance. The disturbances ω_x and ω_y are assumed to be bounded: $\|\omega_x < \infty\|$ and $\|\omega_y < \infty\|$.

Based on model (20), our objective is to design an H ∞ observer for a nonlinear fractional order system for battery SOC estimation.

III. H∞ OBSERVER DESIGN

According to the battery model (20), the following observer is proposed

$$\begin{cases} D^r \hat{x}(t) = A\hat{x}(t) + Bu(t) + L(y(t) - \hat{y}(t)) \\ \hat{y}(t) = C\hat{x}(t) + Du(t) + h\left(\hat{x}(t)\right) \end{cases} \tag{21}$$

where $\hat{x}(t)$ is the state estimation; $\hat{y}(t)$ denotes the output estimation of the real terminal voltage, and L is the observer gain that will be designed later. Then, the error system is given by (22).

$$D^r e_x(t) = A_{cl} e_x(t) + LH\ (t) + (E - LF)\omega(t) \tag{22}$$

where $e_x(t) = x(t) - \hat{x}(t) = \left[\tilde{V}b(t)\ \tilde{V}c(t)\ S\tilde{O}C(t)\right]^T$ is the estimate error of the state; $A_{cl} = A - LC; E = [I_0, 0]$; $F = [0, I_0]; H\ (t) = h\left(\hat{x}(t)\right) - h\ (x(t)); \omega(t) = [\omega_x(t) \omega_y(t)]^{\mathrm{T}}$ is the synthetic disturbance, and I_0 denotes identity matrix with appropriate dimensions.

The aim of designing an H_∞ observer is as follows: For a given attenuation level $\gamma > 0$, designing the observer (21) such that the error system (22) is stable and the following inequality is satisfied under the zero-initial condition

$$\|e_x\ (t)\| \le \gamma\ \|\omega\ (t)\| \tag{23}$$

Since dynamic error system (22) contains fractional order terms, it can not be directly analysed by Lyapunov theory. Hence, continuous frequency integral transformation needs to be applied. To prove the stability of the observer, the following properties and lemmas are presented.

Property 1:

$$H^T(t)H(t) \le e_x^T(t)L_f e_x(t), L_f = diag\left\{0, 0, \beta_{min}^2\right\}$$

Proof: By utilizing the mean value theorem, the following is obtained

$$\begin{aligned} H(t) &= h\left(\hat{x}(t)\right) - h(x(t)) \\ &= -\left.\frac{\partial h}{\partial x}\right|_{x=\xi}\left[(x(t)) - \hat{x}(t)\right] \\ \xi &\in \left[\xi_{V_b(t)} \quad \xi_{Vc(t)} \quad \xi_{SOC(t)}\right]^T \end{aligned} \tag{24}$$

Note that

$$\begin{aligned} \frac{\partial h}{\partial x} &= \left[\frac{\partial h(x(t))}{\partial V_b(t)} \quad \frac{\partial h(x(t))}{\partial V_c(t)} \quad \frac{\partial h(x(t))}{\partial SOC(t)}\right] \\ &= \left[0\ 0\ \dot{h}(SOC)\right] \end{aligned} \tag{25}$$

Then

$$\begin{aligned} H^T(t)H(t) &= e_x^T(t)\left(\frac{\partial h}{\partial x}\right)^T\left(\frac{\partial h}{\partial x}\right)e_x(t) \\ &= e_x^T(t)\begin{bmatrix}0\\0\\\dot{h}(SOC)\end{bmatrix}\begin{bmatrix}0\\0\\\dot{h}(SOC)\end{bmatrix}^T e_x(t) \\ &\le e_x^T(t)L_f e_x(t) \end{aligned} \tag{26}$$

The proof is completed.

Lemma 1: A fractional differential equation, $D^{r_i}x_i(t) = g_i(t), 0 < r_i < 1$, is equivalent to the following continuous frequency distributed model [28].

$$\begin{aligned} \frac{\partial z_i(\omega,t)}{\partial t} &= -\omega z_i(\omega,t) + g_i(t) \\ x_i(t) &= \int_0^\infty \mu_i(\omega)z_i(\omega,t)d\omega \\ \mu_i(\omega) &= \frac{\sin(r_i\pi)}{\pi}\omega^{-r_i} \end{aligned} \tag{27}$$

and for $r_i = 1$, $D^{r_i}x_i(t) = g_i(t)$ can be represented as

$$\begin{aligned} \frac{\partial z_i(\omega,t)}{\partial t} &= -\omega z_i(\omega,t) + g_i(t) \\ x_i(t) &= \int_0^\infty \mu_i(\omega)z_i(\omega,t)d\omega \\ \mu_i(\omega) &= \delta(\omega) \end{aligned} \tag{28}$$

where $g_i(t)$ represents the input; $x_i(t)$ denotes the output; $z_i(\omega,t)$ is the frequency distributed state variable; and $\mu_i(\omega)$ is the frequency weighting function, $\delta(\omega)$ is a unit impulse function.

Lemma 2 [29]: For a matrix S

$$S = \begin{bmatrix} S_{11} & S_{12} \\ S_{21} & S_{22} \end{bmatrix}$$

$S_{12}^T = S_{12}$, if $S_{11} < 0$, $S_{22} - S_{12}^T S_{11}^{-1} S_{12} < 0$ or $S_{22} < 0$, $S_{11} - S_{12}S_{22}^{-1}S_{12}^T < 0$, we must have $S < 0$, and vice versa.

Theorem 1: For the system (20) and the observer (21), with the given attenuation level $\gamma > 0$, if there exist matrices

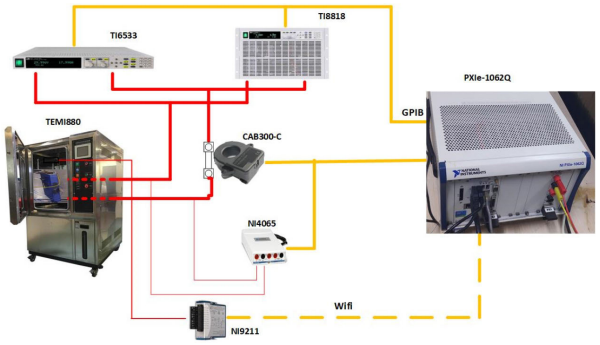

FIGURE 4. Connection diagram of test system.

FIGURE 5. Battery test bench.

$P = P^{\mathrm{T}} > 0$, M with appropriate dimensions, together with a scalar ε, such that

$$\begin{aligned} \Delta &= \begin{bmatrix} \Lambda & M & PE - MF \\ M^T & -\frac{1}{\varepsilon}I & 0 \\ (PE-MF)^T & 0 & -\gamma^2 I \end{bmatrix} < 0 \\ \Lambda &= A^T P + PA - MC - C^T M^T + \frac{1}{\varepsilon}L_f + I \end{aligned} \tag{29}$$

then the error system is globally asymptotically stable at the zero-equilibrium point, where $M = PL$, and the observer gain can be derived by $L = P^{-1}M$.

Proof: According to Lemma 1, (22) can be converted into

$$\begin{aligned} \frac{\partial z(\omega,t)}{\partial t} &= -\omega z(\omega,t) + A_{cl}e_x(t) + LH(t) \\ &\quad +(E - LF)\omega(t) \\ e_x(t) &= \int_0^\infty \mu(\omega)z(\omega,t)d\omega \end{aligned} \tag{30}$$

where

$$\begin{aligned} z(\omega,t) &= \left[z_1(\omega,t)\ z_2(\omega,t)\ z_3(\omega,t)\right]^T \\ e_x(t) &= \left[Vb(t)\ Vc(t)\ SOC(t)\right]^T \\ \mu(\omega) &= diag\left[\mu_1(\omega)\ \mu_2(\omega)\ \mu_3(\omega)\right] \\ &= \begin{bmatrix} \frac{\sin(r_1\pi)}{\pi}\omega^{-r_1} & 0 & 0 \\ 0 & \frac{\sin(r_2\pi)}{\pi}\omega^{-r_2} & 0 \\ 0 & 0 & \delta(\omega) \end{bmatrix} \end{aligned} \tag{31}$$

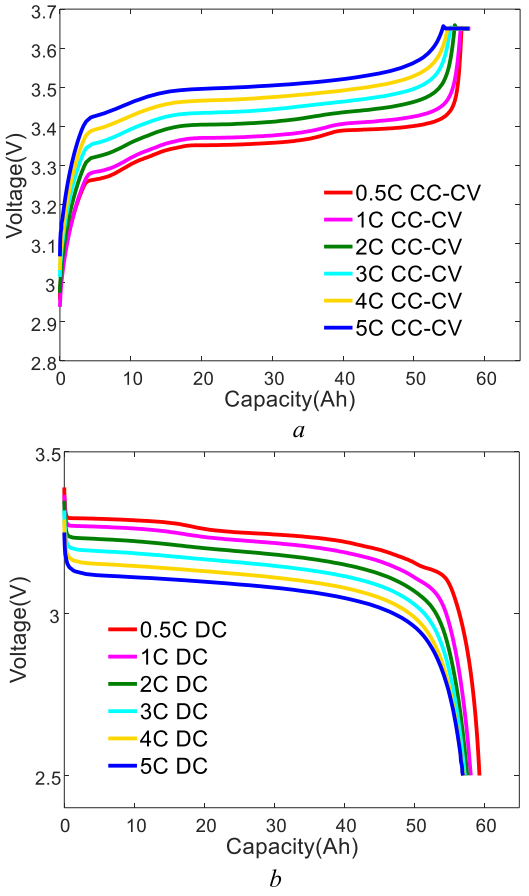

FIGURE 6. Constant current discharge and charge curves at different current rates: (a) constant current charge curve; (b) constant current discharge curve.

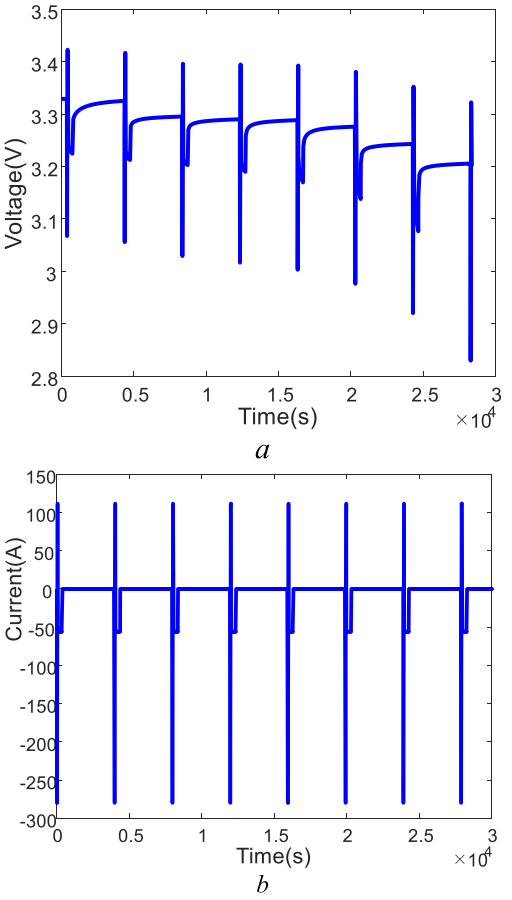

FIGURE 7. HPPC test: (a) voltage profiles; (b) current profiles.

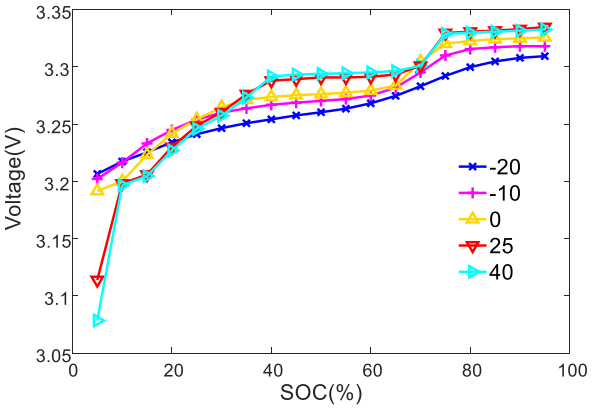

FIGURE 8. OCV-SOC curves at different temperatures.

After the equivalent transformation, the fractional order model is transformed into a continuous frequency distributed state model. In order to analyze the stability of the transformed error system (30), the integral type Lyapunov function (32) is chosen.

$$V(t) = \int_0^\infty z^T(\omega, t)\mu(\omega)Pz(\omega, t)d\omega \tag{32}$$

The derivative of $V(t)$ takes the form of (33), as shown at the bottom of the next page.

To simplify (33), applying Young's inequality [30] to (33) yields

$$\begin{aligned}\dot{V}(t) = {} & e_x^T(t)\left(A_{cl}^T P + PA_{cl}\right)e_x(t) \\ & + \frac{1}{\varepsilon}H^T(t)H(t) + \varepsilon e_x^T(t)MM^T e_x(t) \\ & + \omega^T(t)(E - LF)^T Pe_x + e_x^T(t)P(E - LF)\omega(t)\end{aligned} \tag{34}$$

In addition, according to property 1, (36) is simplified to

$$\begin{aligned}\dot{V}(t) \le {} & e_x^T(t)\left(A_{cl}^T P + PA_{cl} + \frac{1}{\varepsilon}L_f\right)e_x(t) \\ & + \varepsilon e_x^T(t)MM^T e_x(t) + \omega^T(t)(E - LF)^T Pe_x \\ & + e_x^T(t)P(E - LF)\omega(t)\end{aligned} \tag{35}$$

Define the following performance index

$$J = \int_0^\infty \left[e_x^T(t)e_x(t) - \gamma^2\omega^T(t)\omega(t)\right]dt \tag{36}$$

Therefore

$$\begin{aligned}J = {} & \int_0^\infty \left[e_x^T(t)e_x(t) - \gamma^2\omega^T(t)\omega(t) + \dot{V}(t)\right]dt - \int_0^\infty \dot{V}(t)dt \\ < {} & \int_0^\infty \left[e_x^T(t)e_x(t) - \gamma^2\omega^T(t)\omega(t) + \dot{V}(t)\right]dt\end{aligned} \tag{37}$$

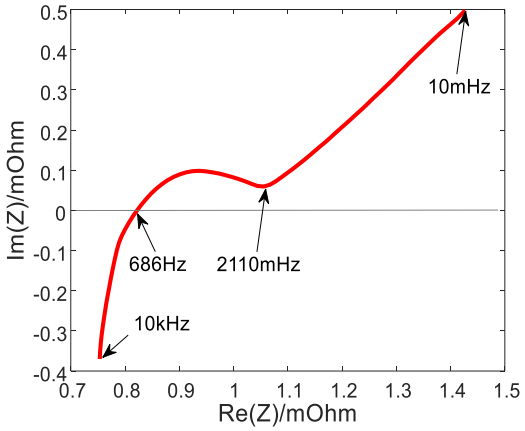

FIGURE 9. EIS of the lithium battery.

A sufficient condition for $J \leq 0$ is that

$$e_x^T(t)e_x(t)-\gamma^2\omega^T(t)\omega(t)+\dot{V}(t)\leq 0, \quad \forall t\in[0,\ \infty) \quad (38)$$

Then

$$\begin{aligned} & e_x^T(t)e_x(t)-\gamma^2\omega^T(t)\omega(t)+\dot{V}(t) \\ & \leq e_x^T(t)\left(A_{cl}^TP+PA_{cl}+\frac{1}{\varepsilon}L_f+I\right)e_x(t) \\ & \quad +\varepsilon e_x^T(t)MM^Te_x(t)-\gamma^2\omega^T(t)\omega(t) \\ & \quad +\omega^T(t)(E-LF)^TPe_x+e_x^T(t)P(E-LF)\omega(t) \end{aligned} \quad (39)$$

By lemma 3, inequality (39) is converted to (40)

$$e_x^T(t)e_x(t)-\gamma^2\omega^T(t)\omega(t)+\dot{V}(t)\leq\begin{bmatrix}e_x(t)\\ \omega(t)\end{bmatrix}^T\Delta\begin{bmatrix}e_x(t)\\ \omega(t)\end{bmatrix} \quad (40)$$

where

$$\Delta=\begin{bmatrix}\Lambda & M & PE-MF\\ M^T & -\frac{1}{\varepsilon}I & 0\\ (PE-MF)^T & 0 & -\gamma^2I\end{bmatrix}$$

$$\Lambda=A^TP+PA-MC-C^TM^T+\frac{1}{\varepsilon}L_f+I \quad (41)$$

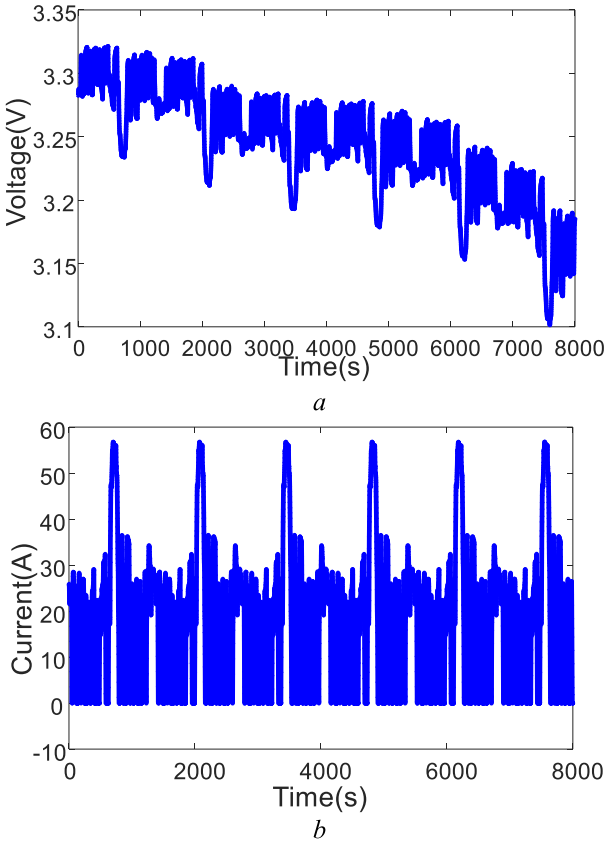

FIGURE 10. Dynamic experiment test: (a) voltage profiles; (b) current profiles.

Therefore, a sufficient condition for $J<0$ is that (41) is less than zero. Then under the zero-initial condition, the following is obtained

$$\|e_x(t)\|-\gamma\|\omega(t)\|\leq 0\Rightarrow\|e_x(t)\|\leq\gamma\|\omega(t)\| \quad (42)$$

This completes the proof.

To realize the above observer, this paper adopts the G-L definition in (4), which is the most direct numerical

$$\begin{aligned} \dot{V}(t) &= \int_0^\infty\left[\frac{\partial z^T(\omega,t)}{\partial t}\mu(\omega)Pz(\omega,t)+z^T(\omega,t)\mu(\omega)P\frac{\partial z(\omega,t)}{\partial t}\right]d\omega \\ &= \int_0^\infty\left[-\omega z(\omega,t)+A_{cl}e_x(t)+LH(t)+(E-LF)\omega(t)\right]^T\mu(\omega)Pz(\omega,t)d\omega \\ &\quad +\int_0^\infty z^T(\omega,t)\mu(\omega)P\left[-\omega z(\omega,t)+A_{cl}e_x(t)+LH(t)+(E-LF)\omega(t)\right]d\omega \\ &\leq \int_0^\infty\left[e_x^T(t)A_{cl}^T\mu(\omega)Pz(\omega,t)+H^T(t)L^T\mu(\omega)Pz(\omega,t)+\omega^T(t)(E-LF)^T\mu(\omega)Pz(\omega,t)\right]d\omega \\ &\quad +\int_0^\infty\left[z^T(\omega,t)\mu(\omega)PA_{cl}e_x(t)+z^T(\omega,t)\mu(\omega)PLH(t)+z^T(\omega,t)\mu(\omega)P(E-LF)\omega(t)\right]d\omega \\ &= e_x^T(t)\left(A_{cl}^TP+PA_{cl}\right)e_x(t)+\omega^T(t)(E-LF)^TPe_x(t)+2e_x^T(t)MH(t)+e_x^T(t)P(E-LF)\omega(t) \end{aligned} \quad (33)$$

TABLE 1. Experiment equipment.

Number	Name	Model	performance index
1	Programmable Digital Multimeter	NI-4065	The range resolution of 10V is 10uV, the worst accuracy in one year is 90ppm (reading) +12ppm (range), temperature drift 5ppm (reading) +1ppm (range).
2	PC	PXIe-1062Q	/
3	Programmable DC Power Supply	ADVICS IT6533	200V/120A/6kW
4	Programmable Electronic Load	ADVICS IT8818	120V/480A/6kW
5	Programmed thermostat	TEMI880	-40℃~+150℃
6	Thermocouple input module	NI-9211	/
7	current sensor	CAB300-C	Sensitivity error < 0.5%, linearity error < 0.1%

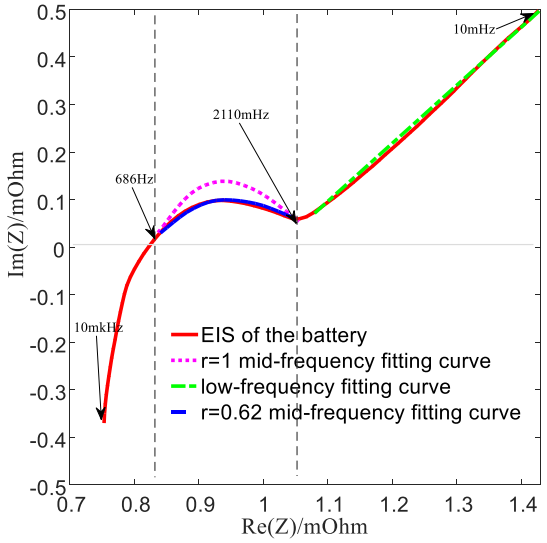

FIGURE 11. CPE order fitting curve.

implementation method.

$$\begin{cases} \hat{x}(k+1) = \left[T_h^r A + diag(r)\right]\hat{x}(k) \\ \quad -\sum_{q=2}^{N+1}(-1)^q \begin{pmatrix} r \\ q \end{pmatrix}\hat{x}(k+1-q) \\ \quad +T_h^r Bu(k) + T_h^r L\left(y(k) - \hat{y}(k)\right) \\ \hat{y}(k) = C\hat{x}(k) + Du(k) + h\left[\hat{x}(k)\right] \end{cases} \tag{43}$$

where

$$\begin{aligned} T_h^r &= diag\left(T_h^{r_1}\ T_h^{r_2}\ T_h\right) \\ \begin{pmatrix} r \\ q \end{pmatrix} &= diag\left[\begin{pmatrix} r_1 \\ q \end{pmatrix}\begin{pmatrix} r_2 \\ q \end{pmatrix}\begin{pmatrix} 1 \\ q \end{pmatrix}\right] \end{aligned} \tag{44}$$

IV. BATTERY TEST SYSTEM AND MODEL PARAMETER IDENTIFICATION

A. BATTERY TEST SYSTEM

According to the actual situation, the connection diagram of test system is shown in Fig. 4. Based on LabVIEW platform, a

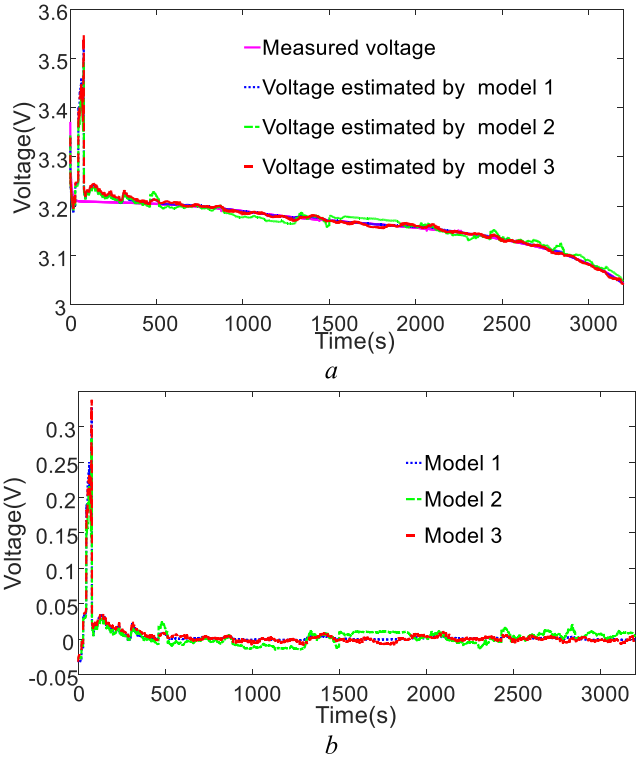

FIGURE 12. The static experiment at 25°C: (a) terminal voltage profiles; (b) terminal voltage estimation error profiles.

battery test bench is built as Fig. 5, the experiment equipment is shown in the Table 1.

The battery used in this paper is lithium-iron phosphate power battery LF56. The characteristic test of battery is be designed, the test consists of six parts: maximum available capacity test, rate characteristic test, hybrid power pulse characterization (HPPC) test, OCV test, AC impedance test and dynamic experiment test.

The purpose of maximum available capacity test is to determine the maximum available capacity of the battery under present situation. The battery is filled with constant current and constant voltage method at standard current, and

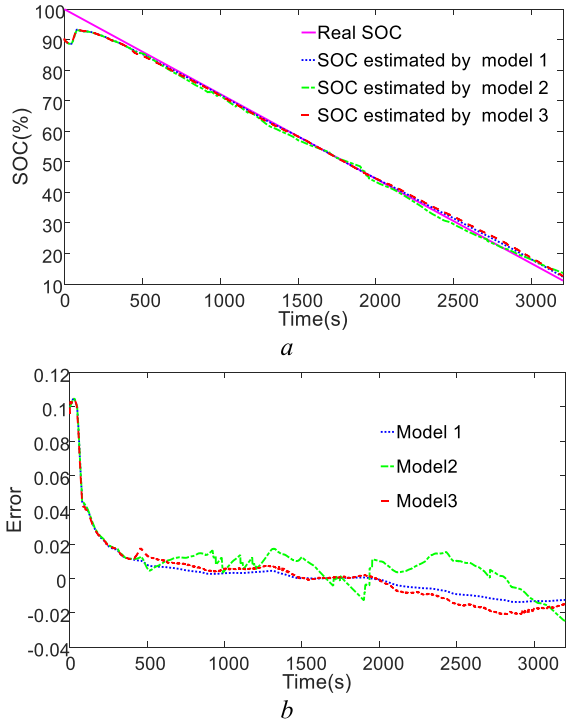

FIGURE 13. The static experiment at 25°C: (a) SOC profiles; (b) SOC estimation error profiles.

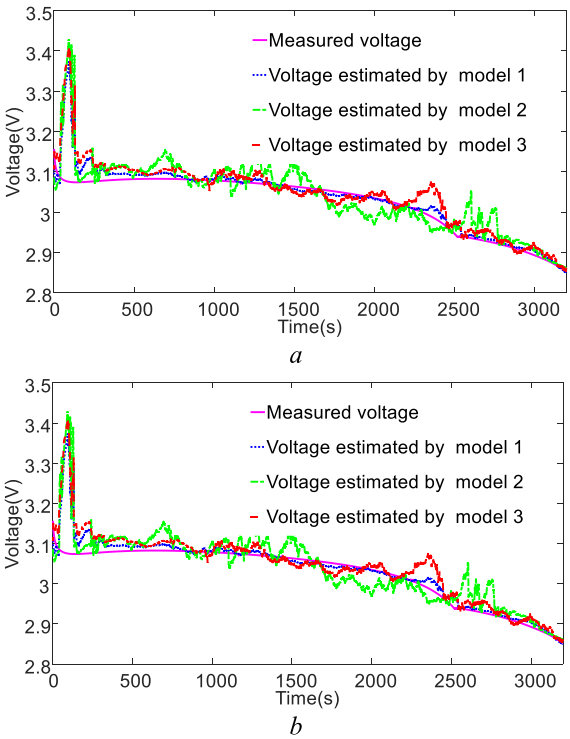

FIGURE 14. The static experiment at −20°C: (a) terminal voltage profiles; (b) terminal voltage estimation error profiles.

then discharged to cut-off voltage with standard current, it is necessary to measure the maximum discharge capacity of the battery for three times and take the average. The maximum available capacity of the battery at different temperatures is shown in Table 2.

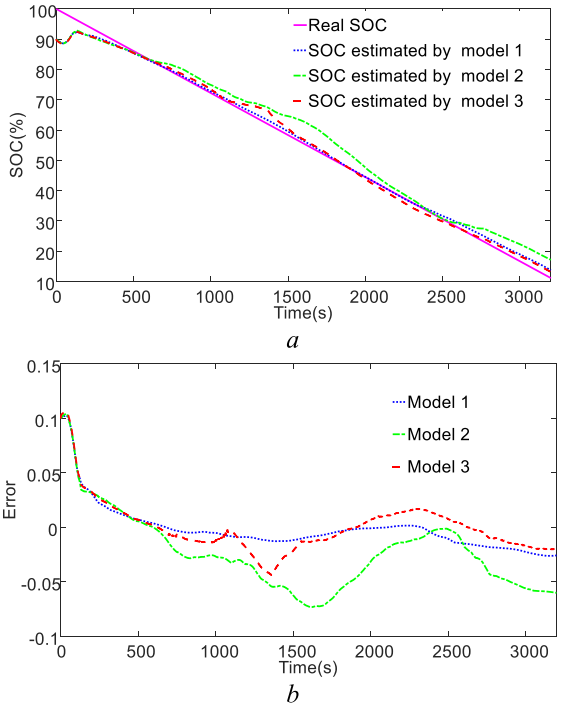

FIGURE 15. The static experiment at −20°C: (a) SOC profiles; (b) SOC estimation error profiles.

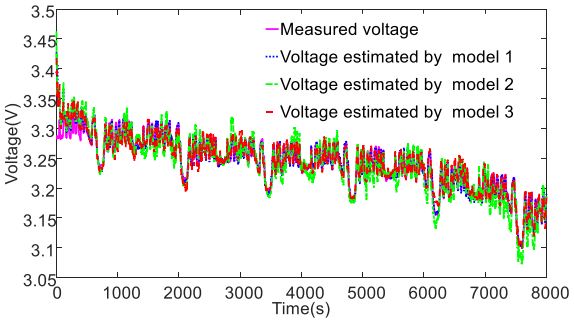

FIGURE 16. Terminal voltage profiles of the dynamic experiment at 25°C.

TABLE 2. Maximum available capacity results at different temperatures.

Temperature /°C	-20	-10	0	25	40
Maximum capacity /Ah	50.05	52.87	54.65	55.92	57.26

The rate characteristic experiment is used to test the capacity retention rate of battery under different charge and discharge direct currents to evaluate the capacity loss of the power battery at high rate. Fig.6 shows the constant current discharge and charge curves of the battery at different direct current (DC) rates.

The HPPC test is used to charge and discharge the power battery by continuous pulse excitation to obtain dynamic characteristics parameters of the power battery, the voltage and current response are shown in Fig.7.

The purpose of OCV test is to establish the relationship between OCV and SOC of power battery. The OCV-SOC curves at different temperatures are obtained through experiments as shown in Fig. 8.

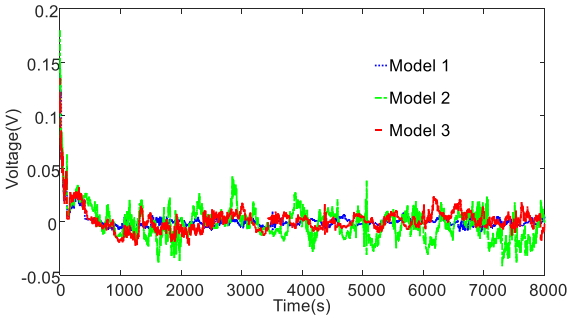

FIGURE 17. Terminal voltage estimation error profiles of the dynamic experiment at 25°C.

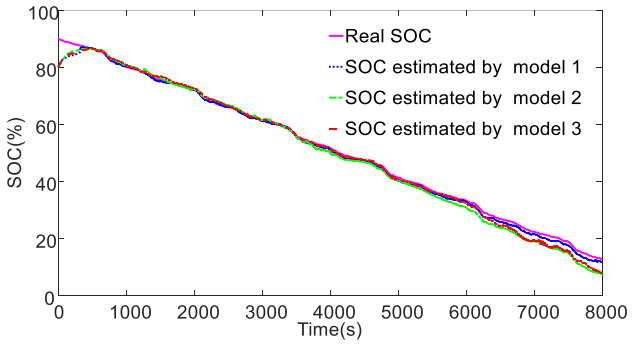

FIGURE 18. SOC profiles of the dynamic experiment at 25°C.

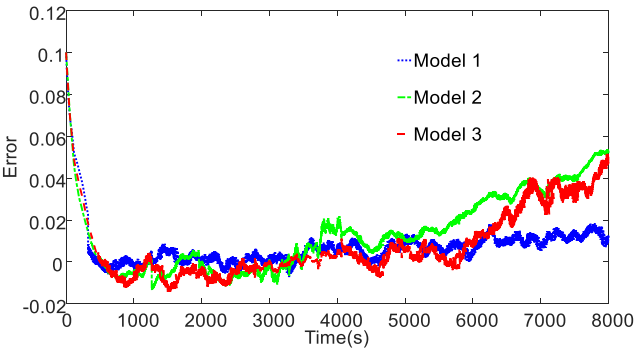

FIGURE 19. SOC estimation error profiles of the dynamic experiment at 25°C.

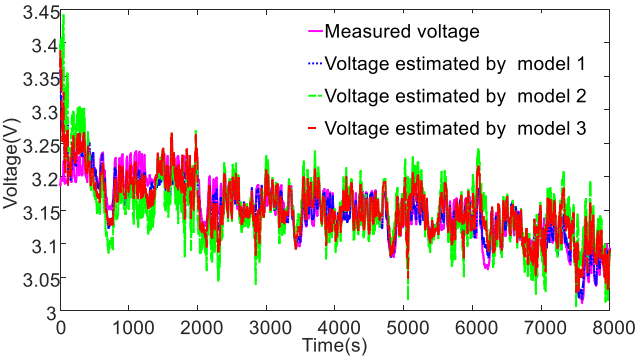

FIGURE 20. Terminal voltage profiles of the dynamic experiment at −20°C.

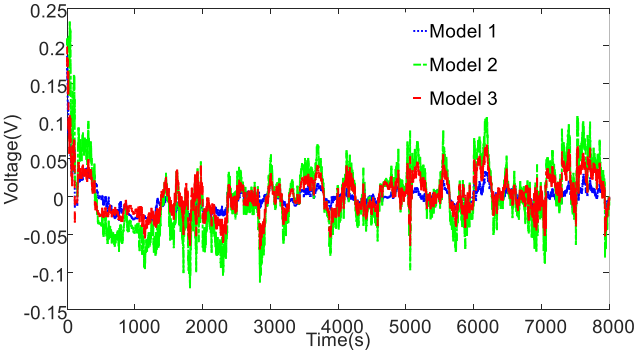

FIGURE 21. Terminal voltage estimation error profiles of the dynamic experiment at −20°C.

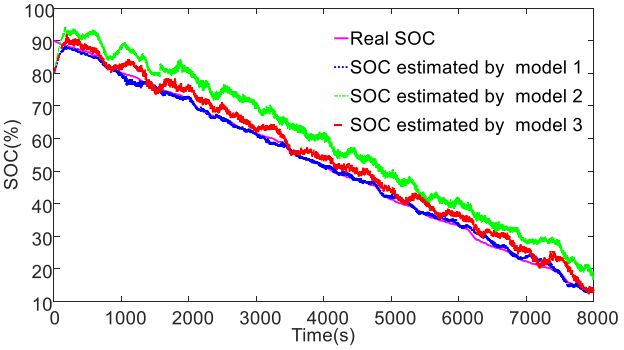

FIGURE 22. SOC profiles of the dynamic experiment at −20°C.

The AC impedance test is a measurement method which uses a small amplitude sinusoidal wave potential as disturbance signal to obtain characterization data of battery related characteristics. Fig.9 shows the measured EIS of battery, the test frequency is 10mHz-10kHz.

The dynamic experiment test is carried out under the excitation condition of variable current, Fig.10 shows the current and voltage curves of the dynamic test of the battery.

B. PARAMETER IDENTIFICATION

In order to realize the designed SOC observer, the model parameters need to be identified, the parameters are identified through the joint analysis of EIS and HPPC experimental voltage response of lithium battery. The order of the CPE is identified by using frequency fitting method in frequency domain [31]: the slope of the low-frequency part of EIS is $r_2\pi/2$ and commonly nearly $\pi/4$, so parameter r_2 is equal to 0.5. The impedance spectrum curve composed of CPE and a resistance is shaped like a semicircle, and the regression rate of the semicircle varies will be changed with r_1, when $r_1 = 0.62$, the measured impedance spectra will be matched well, as shown in Fig.11.

We have performed battery tests at different temperatures (−20°C, −10°C, 0°C, 25°C, 40°C). Due to the length limit of the paper, the simulation and experiment results at −20°C and 25°C are given later. The residual parameters are identified by the least squares method according to the voltage response of HPPC test shown in Fig.7 [31], [32], and the results of parameter identification is shown in Table 3.

TABLE 3. Results of parameter identification.

	k_J	Y_1	Y_2	R_a	R_c
25°C	17.189	107.77×10^3	30.93×10^3	0.82mΩ	0.1531mΩ
-20°C	15.342	94.44×10^3	44.81×10^3	0.84mΩ	0.1646 mΩ

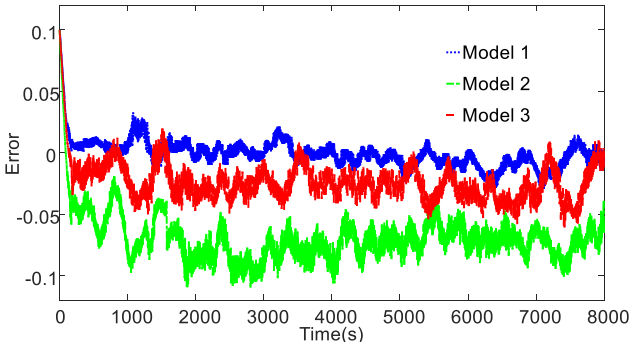

FIGURE 23. SOC estimation error profiles of the dynamic experiment at −20°C.

TABLE 4. Identified coefficients for the OCV-SOC polynomial.

	d_5	d_4	d_3	d_2	d_1	d_0
-20°C	-6.01	13.91	-11.03	3.37	-0.11	3.19
25°C	-11.9	29.36	-25.57	8.97	-0.79	3.18

For the OCV at −20°C and 25°C, the polynomial function fitting method is used to obtain the function of SOC with OCV as shown in (45), and the fitting results are shown in Table 4.

$$h(SOC) = d_5 * SOC^5 + d_4 * SOC^4 + d_3 * SOC^3 + d_2 * SOC^2 + d_1 * SOC + d_0 \quad (45)$$

The LMI toolbox in MATLAB is used to solve the LMIs (29), the observer gains at different temperatures are (46), as shown at the bottom of this page.

V. EXPERIMENT VALIDATIONS OF THE SOC ESTIMATION

The efficiency of the proposed model with nonlinear observer will be verified by both the static and dynamic experimental operating conditions.

Static experiment: the discharging current is set to constant 1C (56A) in the battery testing system, and the experiment are conducted at different temperatures of 25°C and −20°C. The reference SOC curve is calculated based on the ampere-hour integral method. In order to compare the performance of the model, the proposed model in the paper, the integer order model, and the electrochemical impedance model which do not introduce the BV equation are used to predict the output. The above three models are recorded as Model 1, Model 2 and Model 3, respectively.

At 25°C, the terminal voltage estimation and its errors in Fig.12, and SOC estimation and its errors are shown in Fig.13.

At −20°C, the terminal voltage estimation and its errors in Fig.14, and SOC estimation and its errors are shown in Fig.15.

To evaluate the performance of the proposed SOC estimation model, the dynamic experiment shown in Fig.10 is conducted with the proposed SOC estimation model and other two models. At 25°C, the terminal voltage estimation, terminal voltage estimation errors, the SOC estimation and its errors are shown in Figs.16-19, respectively.

At −20°C, the terminal voltage estimation and its errors, the SOC estimation and its errors are shown in Figs.20-23, respectively.

Table 5 and Table 6 are the root mean square error (RMSE), mean absolute error (MAE), maximum error (MAX) of the all models under static experiment and dynamic experiment at −20°C and 25°C. It can be observed that all models perform better at high temperature than at low temperature in Table 5 and Table 6, the RMSE of the proposed model at −20°C and 25°C is smaller than the other two models, this phenomenon is more evident at the lower temperature. It can be seen from Fig.12,14,16 and 20 that the proposed model has less error and higher precision than the other two models in estimating the terminal voltage. Fig.13,15.18 and 22 show that the proposed model can accurately estimate SOC, and the estimation error of SOC is limited to a very narrow error range, the error of the proposed model is less than the other two model after convergence. This shows that the proposed model can estimates battery terminal voltage more accurately, which is used to correct the estimated SOC. It can be observed from Table 6 that when estimating the battery SOC in a dynamic environment, the proposed model is better than the other two models to predict the output. Moreover, at −20 °C where the performance of the other two models deteriorate significantly, the proposed model can still give an accurate SOC estimation with the RMSE less than 0.05.

$$\begin{array}{cc} 25°\mathrm{C} & -20°\mathrm{C} \\ \varepsilon = 0.191\gamma = 1.578 & \varepsilon = 0.245\gamma = 2.491 \\ P = \begin{bmatrix} 1.1424 & -0.0457 & -0.0102 \\ -0.0457 & 1.2613 & -0.0302 \\ -0.0102 & -0.0302 & 1.0812 \end{bmatrix} & P = \begin{bmatrix} 1.1251 & -0.0498 & -0.0015 \\ -0.0498 & 1.2205 & -0.0446 \\ -0.0102 & -0.0446 & 1.0747 \end{bmatrix} \\ L = \begin{bmatrix} -0.2725 \\ -0.1873 \\ -0.2514 \end{bmatrix} & L = \begin{bmatrix} -0.3342 \\ -0.2473 \\ -0.0422 \end{bmatrix} \end{array} \quad (46)$$

TABLE 5. Estimation Performance of Three Models for Static Experiment.

Model		-20°C			25°C		
		RMSE	MAE	MAX	RMSE	MAE	MAX
Model 1	Terminal voltage(V)	0.0454	0.0142	0.2983	0.0176	0.0051	0.2830
	SOC	0.0324	0.0132	0.1041	0.0302	0.0076	0.1049
Model 2	Terminal voltage(V)	0.0946	0.0321	0.3536	0.0408	0.0094	0.3283
	SOC	0.0851	0.0352	0.1111	0.0534	0.0135	0.1050
Model 3	Terminal voltage(V)	0.0856	0.0257	0.3374	0.0304	0.0067	0.3178
	SOC	0.0568	0.0195	0.1058	0.0367	0.0123	0.1051

TABLE 6. Estimation Performance of Three Models for Dynamic Experiment.

Model		-20°C			25°C		
		RMSE	MAE	MAX	RMSE	MAE	MAX
Model 1	Terminal voltage(V)	0.0495	0.0149	0.1867	0.0246	0.0058	0.1450
	SOC	0.0378	0.0143	0.1000	0.0370	0.0078	0.1000
Model 2	Terminal voltage(V)	0.1232	0.0349	0.2324	0.0455	0.0134	0.1799
	SOC	0.2045	0.0706	0.1098	0.0761	0.0183	0.1000
Model 3	Terminal voltage(V)	0.0896	0.0271	0.1989	0.0364	0.0097	0.1350
	SOC	0.0995	0.0311	0.1000	0.0501	0.0141	0.1000

VI. CONCLUSION

Based on the analysis of EIS, a fractional order model of lithium-ion batteries based on electrochemical impedance was proposed, and BV equation was introduced to replace the polarization resistance in conventional equivalent circuit model. An H∞ observer for the SOC estimation is designed. By Lyapunov's direct method, the observer gains which can stabilize the error system are obtained. The experiment and simulation results show that the proposed model and the observer can accurately estimate the battery state.

REFERENCES

[1] J. Li, R. Xiong, Q. Yang, F. Liang, M. Zhang, and W. Yuan, "Design/test of a hybrid energy storage system for primary frequency control using a dynamic droop method in an isolated microgrid power system," *Appl. Energy*, vol. 201, pp. 257–269, Sep. 2017.

[2] R. Xiong, Y. Zhang, H. He, X. Zhou, and M. G. Pecht, "A double-scale, particle-filtering, energy state prediction algorithm for lithium-ion batteries," *IEEE Trans. Ind. Electron.*, vol. 65, no. 2, pp. 1526–1538, Feb. 2018.

[3] Y. Wang, C. Zhang, and Z. Chen, "A method for joint estimation of state-of-charge and available energy of $LiFePO_4$ batteries," *Appl. Energy*, vol. 135, pp. 81–87, Dec. 2014.

[4] R. Yang, R. Xiong, H. He, H. Mu, and C. Wang, "A novel method on estimating the degradation and state of charge of lithium-ion batteries used for electrical vehicles," *Appl. Energy*, vol. 207, pp. 336–345, Dec. 2017.

[5] S. Peng, C. Chen, H. Shi, and Z. Yao, "State of charge estimation of battery energy storage systems based on adaptive unscented Kalman filter with a noise statistics estimator," *IEEE Access*, vol. 5, pp. 13202–13212, 2017.

[6] N. A. Chaturvedi, R. Klein, J. Christensen, J. Ahmed, and A. Kojic, "Algorithms for advanced battery-management systems," *IEEE Control Syst. Mag.*, vol. 30, no. 3, pp. 49–68, Jun. 2010.

[7] Y. Shen, "Adaptive online state-of-charge determination based on neuro-controller and neural network," *Energy Convers. Manage.*, vol. 51, no. 5, pp. 1093–1098, May 2010.

[8] R. Xiong, J. Cao, Q. Yu, H. He, and F. Sun, "Critical review on the battery state of charge estimation methods for electric vehicles," *IEEE Access*, vol. 6, pp. 1832–1843, 2018.

[9] X. Hu, F. Sun, and Y. Zou, "Estimation of state of charge of a lithium-ion battery pack for electric vehicles using an adaptive Luenberger observer," *Energies*, vol. 3, no. 9, pp. 1586–1603, Sep. 2010.

[10] J. Xu, C. C. Mi, B. Cao, J. Deng, Z. Chen, and S. Li, "The state of charge estimation of lithium-ion batteries based on a proportional-integral observer," *IEEE Trans. Veh. Technol.*, vol. 63, no. 4, pp. 1614–1621, May 2014.

[11] I.-S. Kim, "The novel state of charge estimation method for lithium battery using sliding mode observer," *J. Power Sour.*, vol. 163, no. 1, pp. 584–590, Dec. 2006.

[12] I.-S. Kim, "Nonlinear state of charge estimator for hybrid electric vehicle battery," *IEEE Trans. Power Electron.*, vol. 23, no. 4, pp. 2027–2034, Jul. 2008.

[13] F. Sun, X. Hu, Y. Zou, and S. Li, "Adaptive unscented Kalman filtering for state of charge estimation of a lithium-ion battery for electric vehicles," *Energy*, vol. 36, no. 5, pp. 3531–3540, May 2011.

[14] D. Li, J. Ouyang, H. Li, and J. Wan, "State of charge estimation for LiMn2O4 power battery based on strong tracking sigma point Kalman filter," *J. Power Sour.*, vol. 279, pp. 439–449, Apr. 2015.

[15] H. He, R. Xiong, X. Zhang, F. Sun, and J. Fan, "State-of-charge estimation of the lithium-ion battery using an adaptive extended Kalman filter based on an improved thevenin model," *IEEE Trans. Veh. Technol.*, vol. 60, no. 4, pp. 1461–1469, May 2011.

[16] R. Xiong, H. He, F. Sun, and K. Zhao, "Evaluation on state of charge estimation of batteries with adaptive extended Kalman filter by experiment approach," *IEEE Trans. Veh. Technol.*, vol. 62, no. 1, pp. 108–117, Jan. 2013.

[17] Y. Wang, C. Zhang, and Z. Chen, "A method for state-of-charge estimation of $LiFePO_4$ batteries at dynamic currents and temperatures using particle filter," *J. Power Sour.*, vol. 279, pp. 306–311, Apr. 2015.

[18] J. Li, J. Klee Barillas, C. Guenther, and M. A. Danzer, "Multicell state estimation using variation based sequential Monte Carlo filter for automotive battery packs," *J. Power Sour.*, vol. 277, pp. 95–103, Mar. 2015.

[19] F. Zhang, G. Liu, L. Fang, and H. Wang, "Estimation of battery state of charge with H_∞ observer: Applied to a robot for inspecting power transmission lines," *IEEE Trans. Ind. Electron.*, vol. 59, no. 2, pp. 1086–1095, Feb. 2012.

[20] Y. Zhang, C. Zhang, and X. Zhang, "State-of-charge estimation of the lithium-ion battery system with time-varying parameter for hybrid electric vehicles," *IET Control Theory Appl.*, vol. 8, no. 3, pp. 160–167, Feb. 2014.

[21] X. Han, M. Ouyang, L. Lu, and J. Li, "Simplification of physics-based electrochemical model for lithium ion battery on electric vehicle. Part II: Pseudo-two-dimensional model simplification and state of charge estimation," *J. Power Sour.*, vol. 278, pp. 814–825, Mar. 2015.

[22] M. Chen and G. Rincon-Mora, "Accurate electrical battery model capable of predicting runtime and I–V performance," *IEEE Trans. Energy Convers.*, vol. 21, no. 2, pp. 504–511, Jun. 2006.

[23] R. Xiong, J. Tian, W. Shen, and F. Sun, "A novel fractional order model for state of charge estimation in lithium ion batteries," *IEEE Trans. Veh. Technol.*, vol. 68, no. 5, pp. 4130–4139, May 2019.

[24] J. Tian, R. Xiong, and Q. Yu, "Fractional-order model-based incremental capacity analysis for degradation state recognition of lithium-ion batteries," *IEEE Trans. Ind. Electron.*, vol. 66, no. 2, pp. 1576–1584, Feb. 2019.
[25] A. Flores-Tlacuahuac and L. T. Biegler, "Optimization of fractional order dynamic chemical processing systems," *Ind. Eng. Chem. Res.*, vol. 53, no. 13, pp. 5110–5127, Apr. 2014.
[26] I. Petras, *Fractional-Order Nonlinear Systems: Modeling, Analysis and Simulation*. Berlin, Germany: Springer, 2011.
[27] W. Waag, C. Fleischer, and D. U. Sauer, "On-line estimation of lithium-ion battery impedance parameters using a novel varied-parameters approach," *J. Power Sour.*, vol. 237, pp. 260–269, Sep. 2013.
[28] J. Trigeassou, N. Maamri, J. Sabatier, and A. Oustaloup, "A Lyapunov approach to the stability of fractional differential equations," *Signal Process.*, vol. 91, no. 3, pp. 437–445, Mar. 2011.
[29] E. A. Boroujeni and H. R. Momeni, "Non-fragile nonlinear fractional order observer design for a class of nonlinear fractional order systems," *Signal Process.*, vol. 92, no. 10, pp. 2365–2370, Oct. 2012.
[30] F. Chen and W. Zhang, "LMI criteria for robust chaos synchronization of a class of chaotic systems," *Nonlinear Anal., Theory, Methods Appl.*, vol. 67, no. 12, pp. 3384–3393, Dec. 2007.
[31] J. Xu, C. C. Mi, B. Cao, and J. Cao, "A new method to estimate the state of charge of lithium-ion batteries based on the battery impedance model," *J. Power Sour.*, vol. 233, pp. 277–284, Jul. 2013.
[32] Q. Zhu, N. Xiong, M.-L. Yang, R.-S. Huang, and G.-D. Hu, "State of charge estimation for lithium-ion battery based on nonlinear observer: An H∞ method," *Energies*, vol. 10, no. 5, p. 679, May 2017.

NING CHEN received the B.S. and M.S. degrees in industrial electrical automation from the Central South University of Technology, in 1992 and 1995, respectively, and the Ph.D. degree in control theory and engineering from Central South University, China, in 2002. Since 1995, she has been with the School of Automation, Central South University, where she is currently a Professor. Her research interests include modeling and optimal control of complex systems, decentralized control of large-scale systems, and battery management systems.

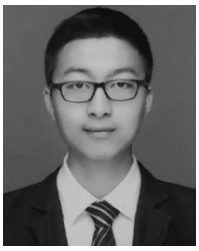

PENG ZHANG received the B.S. degree in electrical engineering and automation from Central South University, Changsha, China, in 2017, where he is currently pursuing the M.Sc. degree in electrical engineering with the School of Automation. His research interests include modeling and state estimation of lithium-ion batteries.

JIAYANG DAI received the B.S. and M.S. degrees in control science and engineering from Central South University, in 2009 and 2012, respectively, where he is currently pursuing the Ph.D. degree. His interests are in soft sensor modeling and optimal control of complex industrial process.

WEIHUA GUI received the B.Eng. and M.Eng. degrees in control science and engineering from Central South University, Changsha, China, in 1976 and 1981, respectively. From 1986 to 1988, he was a Visiting Scholar with Universität-GH-Duisburg, Germany. He has been a Full Professor with the School of Automation, Central South University, since 1991. His main research interests are in modeling and optimal control of complex industrial process, distributed robust control, and fault diagnoses. He was elected as an academician of Chinese Academy of Engineering, in 2013.